Laser and Particle Beams (1991), *vol.* 9, *no.* 1, *pp.* 49–69
Printed in the United States of America

High speed proximity focused X-ray cameras

By J. D. KILKENNY
Lawrence Livermore National Laboratory, University of California,
Livermore, CA 94550, USA

(Received 9 April 1990)

Recent technological developments have resulted in sub 100 ps shutter times of X-ray cameras that are based on the gating of microchannel plates. Moreover, these cameras are reliable enough to be used on large experimental systems. A review is given of the development of gated proximity focused detectors and of the factors affecting their performance.

1. Introduction

In the last five years, there has been a noticeable increase in the shutter speed of high speed gated X-ray cameras. In 1983 the state-of-the-art in open shutter time for X-ray cameras was ~1 ns (Stewart 1983), with the complication of using a short pulse laser as the voltage pulse generator. It is presently <100 ps with systems compact and robust enough that the gating cameras have been routinely and reliably used on several large experimental facilities. The simplicity of the cameras has allowed them to capture several images gated at adjustable interframe times. They have been used as the detector of a 15-frame gated X-ray pinhole camera, as the stripline detector for a crystal spectrometer, and for a grazing incidence soft X-ray grating spectrometer.

The primary application so far of gated X-ray detectors has been in the field of inertial confinement fusion and X-ray laser research. In the first case, the considerations leading to the requirement for sub-100 ps gating come from the need to avoid motional blurring during the exposure of moving and X-ray emitting objects. For laser produced plasmas and ICF the plasma velocity is typically $\sim 10^7$ cm/s, and as the required spatial resolution is less than 10 μm, a shutter time of less than 100 ps is needed to freeze the motion. In X-ray laser research, the gain duration of XUV lines can be short compared to emission time of the laser heated plasma which can radiate for many nanoseconds in the VUV as it cools.

Traditionally, there are two techniques for gating of images, shuttering of image converter electron-optic tubes (Finn *et al.* 1985; Kalibjan & Thomas 1983; Sibbett *et al.* 1982; Hadland 1978; Eagles *et al.* 1986), and the gating of proximity focused devices. In an image converter camera, photons are converted to photo-electrons at a photo-cathode, and a photo-electron image of the photo-cathode is formed on a phosphor by an electron lens (Hadland 1978). Several variations on a basic scheme have been proposed to obtain sub nanosecond gating of electron optic tubes. There is a region of the electron lens where the photo-electrons "cross over," i.e., the electron beam is small. In this region deflection plates apply an electric field normal to the beam direction that sweeps the beam past a second aperture plate. An exposure is obtained when the electron beam is swept across the aperture analogous to the lens plane shutter of an optical camera. (A system analogous to the focal plane shutter of an optical camera has also been used (Kalibjian & Thomas 1983).) To correct for the sideways motion of the e-beam that passes through the aperture, a pair of corrector plates follows the original deflection plates with a compensating deflection.

 0263-0346/91 $5.00 + .00

The traditional problem with this technique is the loss of spatial resolution at short exposure time, especially in the direction of deflection.

Variants on this scheme achieving comparable results have been reported (Finn *et al.* 1985) where a staircase deflection voltage is applied and there is no aperture plate.

Another variant of image tube gating where the switching is at the phosphor has been demonstrated (Hares 1987). A low energy (5 keV) electron image is formed at the phosphor which has an Al over-coating to prevent the 5keV ungated electron image from exciting the phosphor. To gate the camera on an accelerating voltage is applied at the phosphor of ~1 kV to give the electrons enough energy to excite the phosphor.

Image converter tubes can now achieve high temporal and spatial resolution. For example, recently (Sibbett *et al.* 1989) a four frame X-ray converter camera was demonstrated with ~200 ps time resolution at ~6 lp/mm limiting visual resolution. These techniques based on image converter cameras build on the enormous success in the last decade of streak camera technology. Their principal advantage is that several frames of an object viewed along identical lines-of-sight can be obtained from a single X-ray image formed on a single cathode. However, their complexity, the need for a separate intensifier to avoid space charge effects in the tube, their relatively large size (10s of cm) and the success of proximity focused cameras has restricted their routine use to date.

The second technique is the gating of proximity focused cameras. The basic simplicity, together with their higher demonstrated speed and spatial resolution, has allowed them to be developed sufficiently that they are reliable, compact and consequently in routine use. Although a true multiframe camera cannot be built from proximity focused schemes, the proximity focused schemes discussed below can form many images by using many different gated detector areas on one microchannel plate (MCP) with a small degree of parallax (<1–2°).

The gating of proximity focused X-ray cameras is the subject of this review. The factors affecting the gate time and spatial resolution are summarized in Section 2. A review of gated proximity focused detector development until about 1984 is presented in Section 3. About 1984 technological developments allowed a large improvement in the state-of-the-art of gated MCP cameras and work since 1984 on gated MCP detectors is summarized in Section 4. Possible future developments are described in Section 5.

2. Operational principles of proximity focused cameras

2.1 *Simple proximity gating*

The simplest proximity focused gated X-ray camera is shown in figure 1. It consists of a transmission X-ray cathode separated by a distance L from a phosphor. X rays incident on one side of the photocathode produce secondary photo-electrons close to the rear surface of the cathode, and a gating voltage V applied across the photocathode phosphor gap accelerates photo-electrons from the rear of the photocathode into the phosphor.

Spatial resolution in this scheme is maintained only if the sideways thermal emission velocity of the photo-electrons is much less than the velocity acquired across the gap. The spatial resolution is approximately

$$\delta = 4L\left(\frac{V_0}{eV}\right)^{1/2} \tag{1}$$

where V_0 is the initial energy of the photo-electrons (Henke 1981) assumed to be emitted isotropically. For typical values of $V = 1$ kV, $L = 1$ mm and $V_0 = 1$ eV δ is ~130 μm.

https://doi.org/10.1017/S0263034600002330 Published online by Cambridge University Press

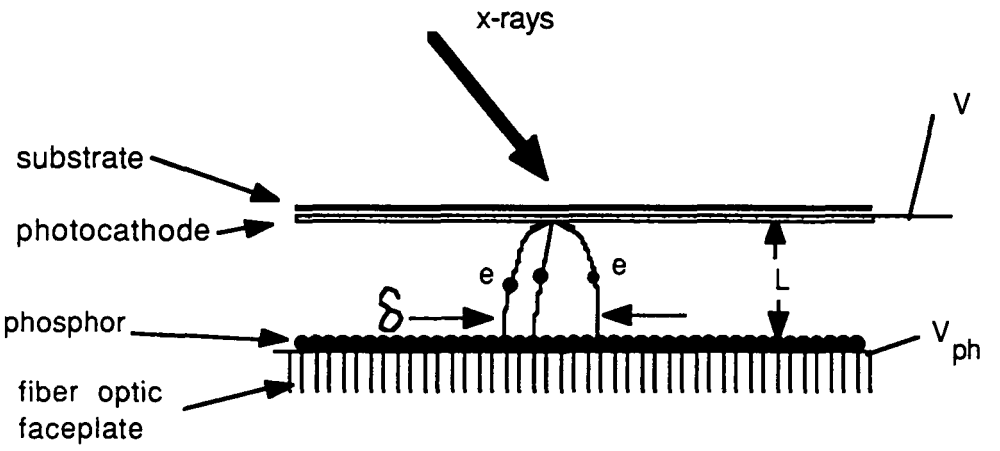

FIGURE 1. Schematic arrangement of the simplest proximity focused camera. The photoelectrons are emitted from the back of the photocathode with a spread in direction, giving rise to the degraded spatial resolution δ at the phosphor as shown.

The electron transit time across the cathode-phosphor gap is important in determining the gate time. For a constant accelerating voltage V, the electron transit time is

$$t_t = \left(\frac{2m}{eV}\right)^{1/2} L \tag{2}$$

typically $V = 1$ kV, $L = 1$ mm, for which t_t is 110 ps.

In a bi-planar vacuum photodiode (displacement) current is detected by the anode during all of the transit of the photo-electrons (Bell 1960), and so the rise time of the diode and therefore the time response is given simply by the electron transit-time across the K–A gap. Although a gating camera resembles a vacuum photo-diode with the phosphor replacing the anode, the difference is that light is emitted from the phosphor only when electrons strike the phosphor. Simplistically one would expect that the gate time of the camera would be

$$t_g = t_v - \left(1 - \frac{1}{2\sqrt{2}}\right) t_t \qquad \text{for } t_v > t_t \tag{3}$$

where t_v is the voltage gate time of the perfect rectangular voltage pulse illustrated in figure 2. If $t_v < t_t$, the photo-electrons will not have the full energy of the gating voltage. As the light output from the phosphor depends on the energy of the incident electron, there would be a consequent reduction in the light output.

In reality the finite rise and fall times of the gating voltage need to be considered. A calculation illustrating the effect of the electron transit time on the gate width is shown in figure 3 for 1 mm cathode–anode gap gated with a 5 kV gating pulse ($t_t = 47$ ps, from eq. 2) having 20 ps rise and fall time, and full width half maximum (FWHM) of 30 ps. Figure 3 shows the energy at the phosphor of photo-electrons "born" at different times during the gating pulse. Because of the 50 ps transit time, only those electrons born during the first half of the gating pulse contribute to the output signal. It can be seen that short gating with $t_g < t_t$ cannot be obtained because of the severe reduction in output signal. One of the first demonstrations of a proximity focused X-ray camera used a simple gating system (Cole 1981), driven by an Auston switch (Auston 1976; Mourou & Knox 1979). Evidence for 100 ps gate times from an X-ray source was obtained.

https://doi.org/10.1017/S0263034600002330 Published online by Cambridge University Press

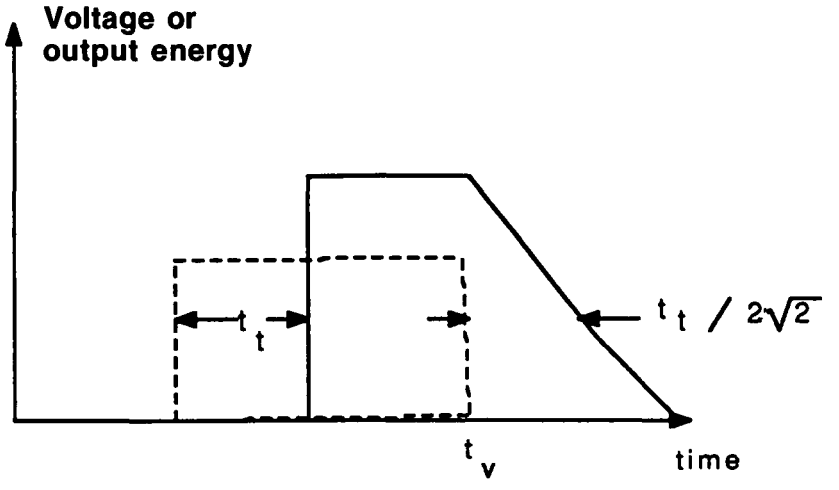

FIGURE 2. The response of a phosphor in a simple proximity focused camera to an idealized square voltage pulse. In contrast to figure 3, the arrival time of photo-electrons at the phosphor is plotted. The decay time of the energy arrival at the phosphor is due to electrons in flight across the photo-cathode-phosphor gap when the voltage is turned off at $t = t_v$.

The main disadvantage of a simple proximity focused scheme is that the cathode has to be thin enough to transmit X rays to its rear surface. These X rays will continue on and excite the phosphor screen leading to a time-integrated image which is fainter than the gated image by the product of the relative efficiency of the phosphor X-ray excitation to electron

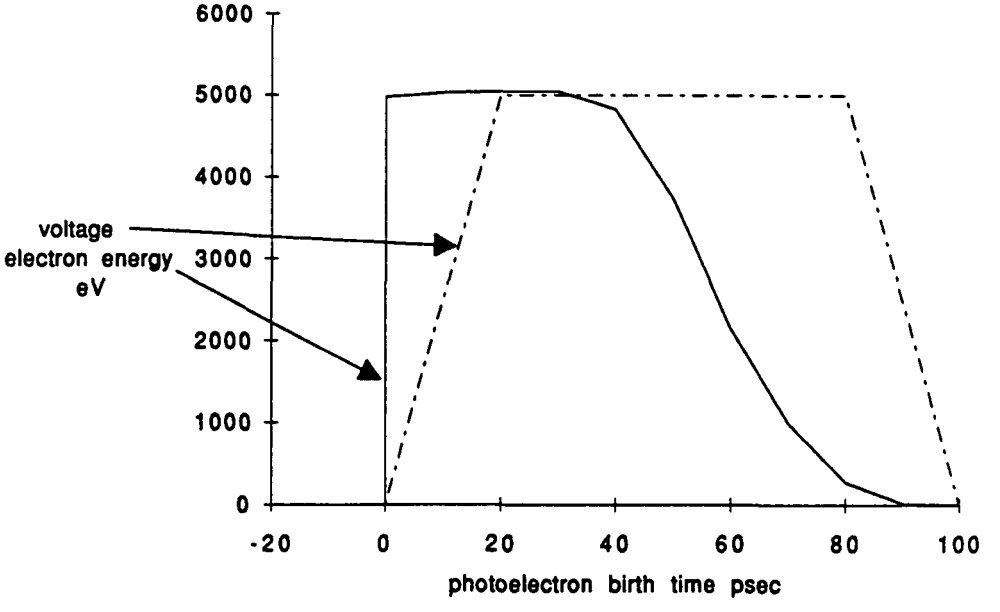

FIGURE 3. Calculations showing the effect of the finite rise and fall time of the voltage on the gating of a proximity focused camera. The 20 ps rise and fall time voltage pulse is shown. The energy in eV electrons at the phosphor is plotted vs their birth time.

https://doi.org/10.1017/S0263034600002330 Published online by Cambridge University Press

excitation and the ratio of the gate width to the emission time of the object. This has the effect of reducing the dynamic range. Another disadvantage is that the gate voltage required can be large with a relatively fast risetime, although such voltages (20 ps risetime, 5 kV into a low impedance) can be produced using photo-conductive "Auston" switches (Auston 1976) driven by a very fast rising laser pulse.

At least two approaches have been used to circumvent the problem of the transmitted X-ray image. One is to separate the electron image from the X rays by drifting the electron image in a magnetic field away from the straight through X-ray image (Dymoke-Bradshaw 1988), and introducing a separate gating electrode close to the photocathode. Limited development work on this approach has demonstrated its viability, but at a severe penalty of complexity. Another approach is to introduce a microchannel plate between the photo-cathode and the detector. If the pores of the microchannel plate are aligned parallel to the photo-electrons, but are angled with respect to the X rays, the straight through X-ray image will not reach the phosphor. This scheme was proposed by Price (1983), but not fully implemented.

A variant on this approach is to bias the pores of the MCP (MCPs are usually supplied with the pores aligned a few degrees off normal to prevent ion feedback) so that X rays are not transmitted but photo-electrons deflected by the self magnetic field of the gating voltage to the MCP bias angle are. By making the camera part of a microstrip line of impedance, $Z_0 = 15\ \Omega$ (Stearns 1989), with an MCP as the ground plane after the anode of the microstrip, and an electron CCD camera after the MCP as a detector, the self magnetic field produced by the Poynting vector of the gating voltage can be used to deflect the photo-electrons. Typical deflection angles are 3.8° for 5 kV pulses with <20 ps rise times.

A high voltage with a fast rising pulse so that $V \neq V(t)$ during the gating is required for the camera. By using a laser trigger and Auston switch with a 20 ps rise time to 5 kV (Stearns *et al.* 1989), gating to 50 ps with good spatial resolution has been demonstrated. To prevent electron buildup in the gap a reverse bias is necessary.

2.2. *Microchannel plate proximity focused cameras*

Microchannel plates, although invented in 1930 (Farnsworth 1930), did not come into everyday scientific use until the late 1960s when they were first developed for Generation II optical intensifiers for night vision applications. In this family of tubes, there is a photocathode from which electrons are accelerated into an MCP that amplifies the photo-electrons, before they are accelerated into a phosphor.

However, in X-ray applications the incident surface of the MCP can be used as the photocathode, with gating and amplification from an applied voltage pulse either across the MCP or the gap between the output of the MCP and the phosphor as illustrated in figure 4. In this scheme, the use of a MCP instead of a vacuum gap as the gating element (cf. figure 1) introduces several advantages:

1) It eliminates the problem of the "DC" image which is blocked by the X-ray attenuation of the MCP.
2) It allows the non-linearity of gain with voltage of an MCP to be exploited resulting in a relaxation of the rise time of the required electrical gating pulse. As high gain occurs for only about 1 kV, the requirement for high voltage fast pulsing is also relaxed.
3) The gain in the MCP eliminates the need for an additional intensifier tube or a very sensitive electron CCD.

To understand these advantages the relevant properties of an MCP are explained below.

https://doi.org/10.1017/S0263034600002330 Published online by Cambridge University Press

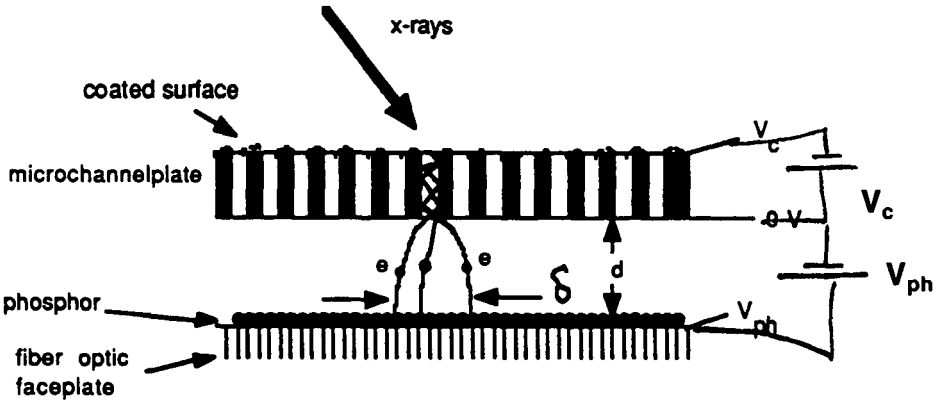

FIGURE 4. Schematic of an MCP X-ray detector. The coating material on the incident surface of the MCP penetrates some distance into the pores depending on the coating angle.

2.2.1. *The use of an MCP as an X-ray detector*

For X-ray use, where simple materials such as gold can be used as a photo-cathode, a coating directly on one side of MCP can be used as a photo-cathode (as shown in figure 4). In this scheme, typical values of the effective quantum efficiency can easily be obtained from calibrations of MCP detectors with a known flux of "DC" X rays as shown in table 1. For a 700 V bias on the MCP, an X-ray flux of 4.2×10^6 photons/cm^2 (at 1.5 keV) gives a charge density on the phosphor of 16×10^{-12} C/cm^2 implying an effective quantum efficiency of 3% from the measured MCP gain of 700.

For normally incident 1.5 keV X rays the quantum efficiency of an Au photo-cathode is ~10% (Henke *et al.* 1981). In MCP use, one expects other angles of incidence on the Au surface coated on the inside of the micropores (Figure 4), but to some degree of approximation, the quantum efficiency will not change (Henke *et al.* 1981). The derived value of 3% is about half of that expected for Au and could be due to the smaller area of the webbing which is 50% of the surface.

The "DC" calibration also allows an approximate comparison with X-ray film. At 700 V MCP voltage, with a 0.7 mg/cm^2 P11 phosphor, a flux of 9.3×10^7 ph/cm^2 at 1.5 keV produces an exposure with optical density (OD) ~1 on Kodak 2484 film. This optical film OD is similar to the film OD that would be obtained from one of the faster X-ray films (e.g., Industrex C), exposed to the same flux of X rays. However, greater film OD can be obtained from the MCP detector by using higher MCP voltages with a gain of a factor of ~3 for every 100 V (at 700 V).

TABLE 1. Typical *DC* calibration of a gold coated MCP at an MCP voltage of 700 V. From the measured MCP electron gain, the effective quantum efficiency of 3% is derived from the X-ray flux and the MCP output charge density

Photon Energy (keV)	X-Ray Flux (photon/cm^2)	MCP Output Charge Density (C/cm^2)	MCP Gain	Effective Quantum Efficiency
1.5	4.2×10^6	16×10^{-12}	700	3%

https://doi.org/10.1017/S0263034600002330 Published online by Cambridge University Press

2.2.2. *Operational model for a microchannel plate gain*

A microchannel plate consists of a matrix of pores in lead glass of diameter D (typically 12 μm on a center–center spacing of 15 μm) with a resistive layer on the inside surface. The resistive layer allows current flow and therefore emission current. Electrons striking the inside surface with energy V_s generate secondary electrons with a gain coefficient (Eberhardt 1979)

$$G_s = \left(\frac{V_s}{V_c}\right)^k$$

where k and V_c are constants dependent on the secondary emission yield.

The simplest model of a microchannel plate is a discrete dynode model, which represents the continuous microchannel plate by n discrete dynodes so that $V_s = V/n$ ($n \gg 1$) where V is the MCP voltage. If the distance between collisions is βD, and is independent of the applied voltage (discussed by Eberhardt (1979)) the total gain in the channel length L is

$$G = g_s^n = \left(\frac{V_s}{V_c}\right)^{nk} = \left(\frac{V}{nV_c}\right)^{nk}.$$

Gain measurements show that $G \propto V^\gamma$ where γ is a constant independent of V, showing that in this respect, the model is consistent with the real devices. Gain measurements of microchannel plates can only give the value of $\gamma = kn$ which for an $L/D = 40$ plate is typically 9. There is disagreement on the value of k: Csorba and Eberhardt (Csorba 1979; Eberhardt 1979) recommend that $k = 1$ and $k = 0.5$ respectively, implying $n = 10$ or $n = 18$. For $L/D = 42$, $G = 1$ is measured at $V = 340$ V and $G = 4200$ at $V = 800$ V. Eberhardt who recommends $n = 18$, therefore obtains $V_c = 22$ V (the voltage at which the gain per stage crosses unity).

For the lead glass used in microchannel plates, the relative permittivity is 8.5 and the ratio of the channel area to the web area is 0.63 giving a capacitance/area of 6.7 pF/cm^2 for a 0.5 mm plate ($L/D = 42$). For 12 μm pores (15 μm spacing), this means the charge stored in the plate capacitance per unit pore at 700 V is 7×10^4 e, where e is the electronic charge.

MCPs do suffer from pulse saturation when enough charge is extracted to change the field at the output end of a pore. The charge available per pore for the final stage of amplification is $\epsilon_r \epsilon_0 DV/(L/D) \sim 60{,}000$ electrons/pore. Non-linearity will occur at lower values, ~10,000 electrons pore (Eberhardt 1979; Leonov *et al.* 1980). This value of maximum gain limits the dynamic range.

For pulsed operation, the recharge time through the typically 2×10^8 Ω of the plate wall is long (~ms) and can be neglected.

In contrast to microchannel plates, the saturation level of channel multipliers can be limited by space charge effects of the electrons in the channel, because of the much larger area of the channel (Schmidt & Handee 1966). But for an MCP, the smaller value of D (10 μm compared to 1000 μm) gives a value of λ ($\pi R^2 \rho$ in Schmidt and Handee (1966)) about 10^{-11} C/m so that only secondary electrons emitted with energy less than 0.1 eV are affected by the space charge in the channel.

2.2.3. *Transit time*

With an applied voltage V across the thickness of a plate, the time between collisions is

$$t_d = \left(\frac{2m}{eV}\right)^{1/2} \frac{L}{n^{1/2}}.$$

https://doi.org/10.1017/S0263034600002330 Published online by Cambridge University Press

If βD is the distance between collisions, then $n = L/\beta D$ and so the *total* transit time in an MCP is

$$t_{tr} = \left(\frac{2m}{eV\beta}\right)^{1/2} L\left(\frac{L}{D}\right)^{1/2}. \tag{4}$$

Typically $L/D = 42$, $V = 800$ V, $\beta = 2$, $L = 0.5$ mm, giving $t_{tr} = 270$ ps.

A transit time spread arises from the fact that secondary electrons are emitted from the inner surface of the pores with a distribution of energies and directions. If the average emission energy is V_o then the time between collisions becomes

$$\beta D\left(\frac{2m}{eV_s}\right)^{1/2}\left(1 \pm \left(\frac{V_s}{V_o}\right)^{1/2}\right)$$

if $V_o \ll V_s$. With n stages, and assuming Poissonian statistics the fractional spread in the transit time is

$$\frac{\delta t_{tr}}{t_{tr}} = \left(\frac{V_o}{nV_s}\right)^{1/2}$$

which for $V_o \sim 8$ eV, $V_s = 22$ V, $n = 18$ is 15% of the total transit time.

This has been modeled by Ito *et al.* (1984) and transit time spreads of ~60 ps (compared to transit times of 300 ps) result. Measurement of the rise time of single hit photomultipliers confirm this effect.

2.2.4. *Response of a gated microchannel plate detector to a pulsed accelerating voltage*

First consider a time-dependent voltage $V(t)$ applied to an MCP where the electron transit time is small compared to $V/(dV/dt)$. In these ideal conditions, the DC model of gain can be used where the gain G is given by

$$G = G_o V^{\gamma}.$$

For a Gaussian time dependent pulse of FWHM $2t_{1/2}$

$$V(t) = V_o \exp - [\ln 2(t/t_{1/2})^2]$$

then

$$G(t) = G_o V_o^{\gamma} \exp - [\ln 2(\gamma^{1/2} t/t_{1/2})^2] \tag{5}$$

i.e., the FWHM of gain is $2t_{1/2}/\gamma^{1/2}$ and as $\gamma \approx 9$–10 for an $L/D = 40$ MCP, the gating FWHM is about one third the voltage FWHM. This sharpening of the pulse response comes directly from the non-linear dependence of gain on voltage. The gain narrowing factor depends on the pulse shape, being greater for a triangular shape where the FWHM of gain is reduced by 7.5, and less for a flat topped voltage pulse which exhibits no gain narrowing.

This simple approach is only true if the transit time is small compared to the electrical gate width $2t_{1/2}$. For an $L/D = 40$, $D = 0.5$ mm plate the electron transit time is ~270 ps so the simple reduction in gate width predicted by eq. (5) would be incorrect for electrical gate widths less than ~300 ps, i.e., shutter gate widths less than about 100 ps.

To model the dependence when the transit time is not negligible, a time-dependent discrete dynode model was used. Here the gain per stage is given by

$$g(t) = (V(t)/nV_c)^k.$$

https://doi.org/10.1017/S0263034600002330 Published online by Cambridge University Press

The transit time between dynodes is then simply (with $t_d \ll [(d/dt)\ln V(t)]^{-1}$)

$$t_d(t_i) = D\left(2\,\frac{L}{D}\,\frac{L}{Dn}\,\frac{m}{e}\,\frac{1}{V(t_i)}\right)^{1/2}$$

where t_i is the time at which the photoelectrons are passing through dynodes i-1 and i. The total gain from a single photoelectron formed at initial time t_{in} is then

$$G(t_{in}) = \prod_{i=1,n} g\left(t_{in} + \sum_{1,i} t_d(t_i)\right).$$

Specific values used are taken from Eberhardt (Eberhardt 1979). Fortunately, in the calculations there seems little sensitivity to the value used for n between 18 and 12; the values used here are $L/D = 40$, $n = 19$, $V_c = 21.8$ V, $k = 0.5$, $D = 12.5$ and 6.25 μm.

It should be emphasized that this model does not take into account the spread in the transit time due to each electron taking slightly different paths.

2.2.5. *Results of calculations and experiments of the pulsed response of an MCP*

The calculated gain as a function of initial time of an $L/D = 40$, $D = 12.5$ μm MCP is shown in figure 5 for a 1100 V gaussian pulse of FWHM 200 ps. The gain is normalized to the DC gain at the peak voltage which occurs at $t = 0$. When plotted as a function of initial time, the gain curve shows the way the gain varies for a single photoelectron liberated at the various initial times along the abscissa, illustrating the X ray response of the camera. The peak gain occurs for photo-electrons born about half an electron transit time before the peak voltage: for the case in figure 5, an electron liberated at -100 ps at the front of the MCP produces an amplified pulse of electrons at the back of the MCP at 99 ps. The FWHM of the gain is 90 ps, narrower than the voltage pulse because of the nonlinearity, but not as narrow as $t_{\mathrm{FWHM}}/9^{1/2}$, the limit in the case of negligible electron transit time (sec. 2.2.4).

For the case of figure 5, the transit time is 220 ps compared to the 200 ps voltage pulse and so the peak normalized gain is only ~0.1. Making the FWHM of the voltage pulse shorter than t_{tr} drastically reduces the gain. However, a 400 V bias in the calculation increases the normalized gain very effectively. The gain FWHM of the MCP is plotted vs the voltage FWHM in figure 6, with the peak normalized gains written on the points. As can be seen, making the FWHM of the voltage pulse shorter than 250 ps, e.g., 167 ps, hardly reduces the gain FWHM, but drastically reduces the peak gain.

Increasing the pulse voltage beyond $V = 1200$ V would be slightly beneficial because the electrons get through the channels more quickly, as $t_{tr} \propto V^{-1/2}$, but is precluded because channel saturation effects would occur.

Bias voltage has a large effect on the peak gain, but little effect on the FWHM. At the shorter voltage FWHM it has the effect of turning the plate on as can be seen by comparing figure 5 without bias to the cases in figure 6 with 400 V bias. The peak normalized gain increases from 0.1 to 0.4. Bias is effective, it is used to adjust gain and it reduces problems with pulse generation. However, there is a possible problem with pulse fidelity through the blocking capacitor that is necessary for a bias. Experimental measurements of the gain FWHM have been made (Power 1988; Bell 1989) as shown on figure 6, corroborating this model.

2.2.6. *Results of calculations with thinner MCPs*

The value of transit time t_{tr} (eq. 6) decreases with the length L of the channel, and MCPs with $D = 6.25$ μm (and still $L/D = 40$ so that the gain does not change) are now com-

https://doi.org/10.1017/S0263034600002330 Published online by Cambridge University Press

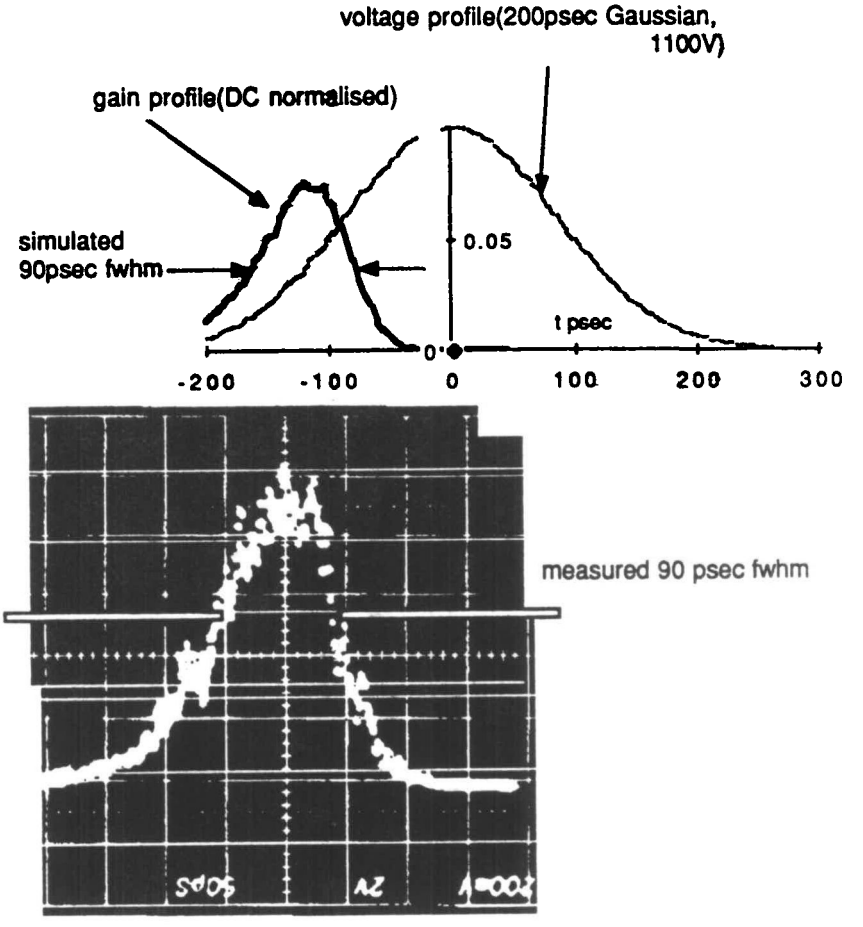

FIGURE 5. The gain as a function of "birth time" for a 200 ps, 1100 V FWHM Gaussian pulse centered at $t = 0$. The gain is normalized to the "DC" gain for the peak voltage of 1100 V. The FWHM of gain is narrower than the voltage FWHM, but wider than predicted by eq. 5. A measurement of the gain FWHM is also shown, exhibiting good agreement.

mercially available. The gain FWHM of these plates together with the peak normalized gain are plotted on figure 6 for the standard 800 V pulse on top of a 400 V bias. A 120 ps FWHM voltage pulse gives 55 ps FWHM of gain. Preliminary experimental results have demonstrated the validity of this model (Kilkenny 1989). Optical photo-multipliers using $D = 6$ μm MCP are available, and in the photo-multiplier configuration give rise to voltage rise times of 150 ps (Kume *et al.* 1988).

In an MCP camera these plates have the advantage of improved spatial resolution, at the price of increased capacitance (lower impedance) and higher drive power.

2.2.7. *Spatial resolution of an MCP detector*

The spatial resolution of an MCP detector is usually set by the spreading between the MCP output and the phosphor, which is normally large compared to the typical 12 μm pore size of MCP. The spatial resolution is

https://doi.org/10.1017/S0263034600002330 Published online by Cambridge University Press

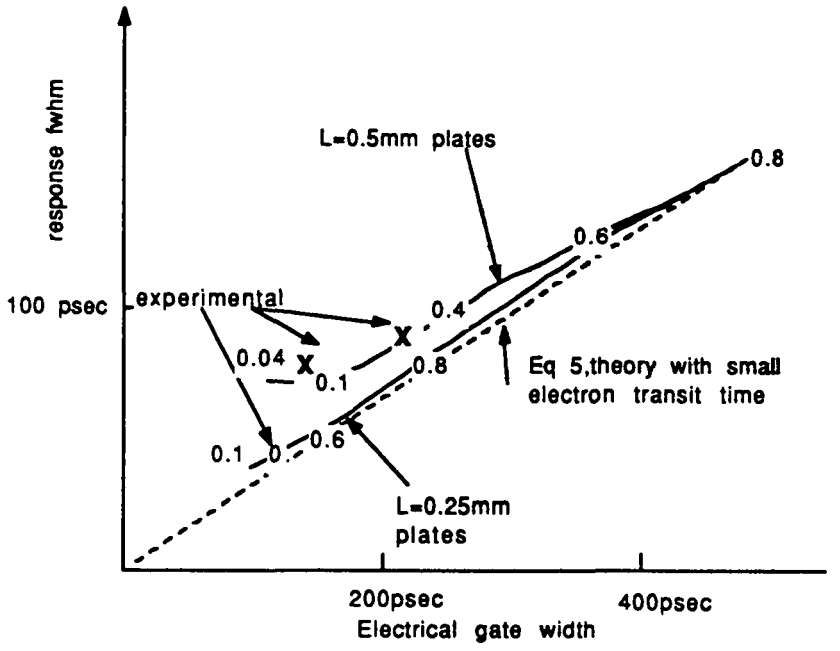

FIGURE 6. The calculated gain FWHM vs the voltage FWHM for 800 V Gaussian pulses with a 400 V "*DC*" bias on a $L/D = 40$ MCP. The values of the peak gain normalized to the "*DC*" gain at the peak voltage of 1200 V are written on the point. The line predicted by eq. 5 for a case with negligible transit time is also shown. Two cases with $L/D = 40$ are shown: $D = 12.5$ μm, $L = 0.5$ mm and $D = 6.25$ Mm, $L = 0.25$ m. Experimental data are shown for the two cases.

$$\delta = 4d\left(\frac{V_o}{eV_{ph}}\right)^{1/2} \tag{6}$$

where V_{ph} is the phosphor voltage with respect to the (grounded) MCP output face, and V_o is the sideways spread in energy of the electron emitted from the MCP and d is the gap between the MCP output and the phosphor. Experimental measurements of the MTF of an MCP detector are shown in figure 7. The 40% contrast appears at 10 lp/mm implying a point spread width of ~40 μm. Other measurements have shown that at low contrast objects as small as 30 μm can be seen. When compared to eq. 6, the measurements suggest that V_o is a few eV.

There can be a significant improvement in spatial resolution depending on the end spoiling w, i.e., how far the conductive coating material is coated into the pores. The value of w is increased by coating the gold more parallel to the direction of the pores of the MCP, and is given by simple geometry. The output energy distribution in the direction normal to the face of an MCP has been measured (Koshida 1985, 1986) and is typically ~30 eV, in contrast to V_o in eq. 6. As the depth of end spoiling w increases from $w = 1.5$ D to $w = 2D$, the number of electrons with emission energies >30 eV decreases, essentially because there is a longer region of micropore where the electric field is small.

A more significant effect is the collimation that the end spoiling produces. The low secondary emission from the end spoiling conductor and the low electric field ensures that the end spoiling region acts as a collimator for electrons. This end spoiling with $w = 2$ D would restrict the maximum emission angle of electrons to be $\tan^{-1}$ 0.5.

The reason larger values of end spoiling are not used is the significant loss in gain as the

https://doi.org/10.1017/S0263034600002330 Published online by Cambridge University Press

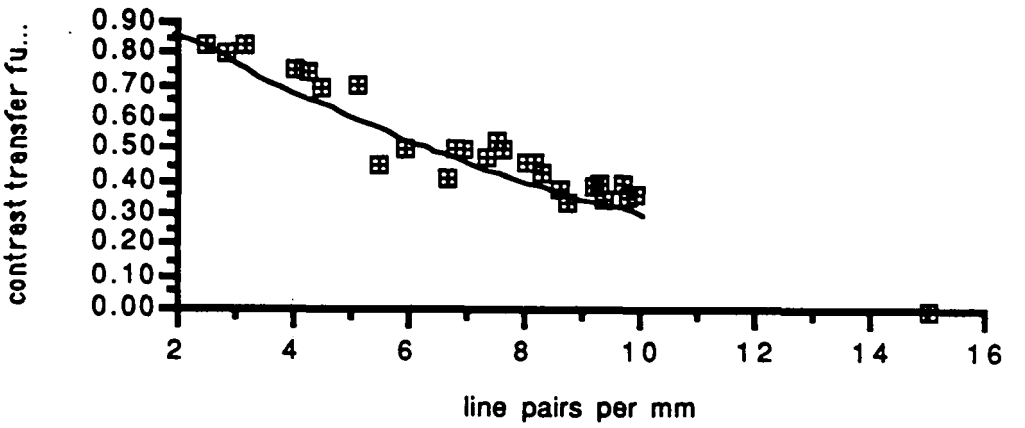

FIGURE 7. The contrast function of an MCP detector as a function of spatial frequency. The measurement was made by a "*DC*" calibration source and a square wave resolution grid.

effective aspect ratio is reduced from L/D to $(L-w)/D$, and more importantly the increased difficulty in extraction of electrons due to the low field at the output side.

2.2.8. *Electrical properties of the MCP coating*

The bulk material of an MCP is glass, an insulator. To provide a conductive surface, the inner surface of the micropores is made "conductive" so that electrical currents ~1 μA flow in cm scale MCPs. The voltage is applied to the MCP by conductive layers coated onto the surface of the MCP. Early MCP detectors (section 3) used the inconel coating, normally ~25 Ω/square to make electrical contact, with a resulting RC charging time of about 1 ns. This is eliminated when the conducting electrodes are coated directly onto the MCP, so that the capacitance of the MCP is "distributed" into a transmission line.

A trade-off must be made in the thickness of the gold coating on the input face (Power & Bell 1988). As the coating thickness is reduced, the detector sensitivity increases because the spoiling decreases, but the resistance of the electrode becomes appreciable. If a microstrip line of width W is coated on the MCP, the characteristic impedance is approximately

$$Z_o = \frac{1}{\sqrt{\epsilon_r}} \frac{L}{W} \sqrt{\frac{\mu_o}{\epsilon_o}}.$$

For Corning 8161 glass ϵ_r = 8.3–8.5 (Wiza 1979), but this is effectively reduced by the open area ratio. For example, 12 μm pores with 15 μm center-to-center spacing give a 63% open area ratio and an effective $\epsilon_{r_{\text{eff}}} = 3.7$, and a calculated group velocity $c/\sqrt{\epsilon_{r_{\text{eff}}}} = 1.5$ cm/100 ps, agreeing with measurements. For the usual L = 0.5 mm thick MCP, 25 and 12.5 Ω impedance microstrips results from coatings of width W 6.4 and 15 mm, respectively (Wheeler 1977). The disadvantage of an MCP over a simple cathode-phosphor proximity focused camera is that the high value of $\sqrt{\epsilon_{r_{\text{eff}}}}$ implies twice as much power compared to a vacuum gap to switch a given detector area.

For a length l of microstrip line, the resistance is

$$R_s = \frac{l\eta}{Wt}$$

https://doi.org/10.1017/S0263034600002330 Published online by Cambridge University Press

where t is the thickness of the surface coating and η is the conductor's resistivity. The fractional voltage loss is then approximately

$$1 - \frac{R_s}{Z + R_s} \simeq \frac{R_s}{Z} = \frac{l\eta}{Lt} \frac{\sqrt{\epsilon_r}}{377} \simeq 0.1$$

for $L = 0.5$, $l = 40$ mm and gold as the coating, and assuming that t, the thickness of the conductor, is less than the electrical skin depth. (This ignores the "swiss cheese" effect of the coating penetrating into the pores both sides of the MCP.) For Au the thickness that is now used is 0.2 μm, but better performance can be obtained with a Cu coating.

The switching voltage on the strip line coated on an MCP propagates at a velocity ~1.5 cm/100 ps. If an image were large compared to the distance the voltage pulse propagates during the gate time different parts of the image would be recorded at different times. Fortunately, this is not generally the case for imaging applications where a typical image size of 5 mm is swept by a voltage pulse in 33 ps. For applications in spectral gating where, for example, a spectrum of a McPig spectrometer could be 20 cm long (Matthews 1985) this is not true, and the time difference along the length of the spectrum must be allowed for. Moving the X-ray angle of incidence away from normal so that the X rays become more parallel to the voltage pulse ameliorates this effect, but cannot remove it because the electrical propagation velocity is less than c.

3. A review of earlier gated proximity focused cameras

The gating of proximity focused imaging tubes was not actively pursued until the need for nanosecond and faster gating arose in the mid 1970s. One of the first applications was on a plasma focus (Nahrath *et al.* 1976, 1979). In this application, a relatively slow voltage pulse (7 ns, 7 kV) was resistively divided in the ratio of 1:4.7 and applied between the input and output of the MCP and also the output of the MCP and the phosphor. In this application, each surface of the MCP was plated with 80 ohm/square inconel (Wiza 1979), through which the capacitance of the MCP was charged, and therefore limiting the response time. With the plate capacitance of 5 pF (40 mm plate; $L = 0.5$ mm) there was an RC charging time of 5 ns. Nevertheless, because of the shortening of gate times from the non-linear gain variation (Section 2) X-ray gate times of ~3 ns were obtained, resulting in beautiful pictures of the hydrodynamic instabilities in a plasma focus.

An interesting variant of this was used in an environment with a very high electrical noise (Fehl 1980). In this camera, which provided five frames of X-ray images, the gating action arose from applying −1 to −1.5 kV 10 ns pulses from a KN22 krytron pulser to 5 separate MCPs ($L/D = 47$, $L = 1.8$ mm) each being 19 mm square. The novel aspect of this camera was a magnetic guide lens relaying the image from the MCP output to a second MCP that had a DC voltage on it. The calculated time-resolution resulting from the non-linear gain shortening the voltage FWHM was 2 ns, although no consideration seems to have been given to RC charging effects of the plate.

A series of papers considering the gating of optical intensifiers highlighted the problem of charging time (Yates *et al.* 1986; Jacoby *et al.* 1983). In an optical shutter tube, attempts to apply a fast rising voltage between the photocathode and phosphor were retarded by the resistance of the cathode substrate. By making special sealed off tubes with a nickel substrate to the photocathode (Yates 1986) this problem could be circumvented. With this improvement, the gate time is then normally limited by the lead inductances (or equivalently, the impedance mismatch) necessary in a sealed off image converter tube.

One solution to the problem caused by the high resistance of the coating on the MCP was used by Fleurot (1982). In this design, a pulsed voltage is applied between a 10 μm Au

coated Be foil photocathode, and an Al covered P11 phosphor. The Be is coated with 0.35 μm of gold which is directly in contact with the input of an MCP. The voltage division across the MCP and the gap between the MCP output and the phosphor is in the ratio of their capacitances, i.e., 1:5.5. The charging time is not limited by the ohmic resistance of the MCP. The disadvantage of this mode of switching is that a 6.5 kV 50 Ω fast rising pulse is required. This was produced by a laser triggered spark gap, producing a rise time of 0.15 ns and a fall time of 0.3 ns. The camera was tested with an X-ray source from a laser produced plasma and gave shutter times in the range of 300–400 ps with a resolution of 6–10 lp/mm. However, laser triggered spark gaps are difficult to use principally because of the jitter. Additionally, the MCP used in this work had a very long transit time.

A significant advance in gating technology which avoided the problem of charging the MCP was described by Stewart *et al.* (1983). In this camera a DC voltage was applied to an MCP with gold coating on both sides but a pulsed voltage of as short as 1.5 ns, 4 kV was applied between the MCP output and a 60% transparent, 500 l.p.i. electroformed grid which was glued to the P11 phosphor. The output of the MCP was coated with 1 μm of Au and configured with six parallel microstrip lines on the phosphor, forming six 50 Ω transmission lines. The rate at which the voltage was applied to the gap depended on the velocity of transmission of the voltage wave along the vacuum strip line. For the nanosecond gate time over the 40 mm active area, this voltage propagation time was negligible, compared to the 1.5 ns rise time of the electrical pulser.

The spatial resolution of the camera was about 50 μm (FWHM). This is consistent with the spreading expected from an MCP output electron energy of 30 eV spread over 20°, crossing the 500 μm gap between the MCP output and the phosphor.

The quoted temporal resolution was less than 1 ns. The temporal degradation is due to the spread in electron transit time through the MCP which for an ideal pulser was less than 40 ps. However, this gating system can suffer from channel saturation leading to a negative image, because the MCP is turned on DC and bright areas of the X-ray image will deplete the gain of the corresponding part of the MCP. MCP recharging times are very long compared to 1 ns time scale of images and so when the MCP output–phosphor gap is pulsed on, this area has a lower gain than the rest of the image.

4. Recent gated proximity focused cameras

The work of Stewart led experimentalists to two important innovations, which within a few years allowed researchers to routinely obtain sub 100 ps gated X-ray images. These innovations were to coat a microstrip transmission line directly onto the MCP (2.2.8.), and to develop electrical gating from the avalanche breakdown of reverse biased *p-n* junctions.

An example of the use of a microstrip coated MCP is given by Young (1986). A 25 Ω impedance line on an MCP was formed by coating a 3 mm wide strip of 2000 Å of Au at a 10° deposition coating angle onto an $L = 0.5$ mm, $L/D = 42$ MCP. The MCP output face was uniformly coated at 45° with 2000 Å of Au. The output electrons were accelerated by a DC voltage onto the phosphor at several kV.

This camera was tested using a laser produced plasma. Part of the 100 ps laser pulse was incident on an Auston switch producing a very fast electrical gate pulse with a 90 ps rise time to 900 V and an FWHM from 180 ps to 250 ps. An electron-transit time of 150 ± 35 ps at 800 V resulted. A variant of this camera was used in a grazing incidence X-ray spectrometer (Matthews 1985) where a DC voltage was applied across an MCP, and the voltage was switched off so that late time X-ray signals were not recorded.

The second important innovation in gating has come from the use of the avalanche breakdown of reverse biased Si *p-n* junction. The avalanche effect at high voltage of re-

verse biased Si *p-n* junction was first published in the West in 1981 (Grekhok 1981). In this work, a steepening of a kilovolt voltage pulse from a 3 ns rise time to ≤1 ns was demonstrated. Subsequent work at LLNL (Booth 1983; Benzel & Pocha 1985) demonstrated that the avalanche breakdown time of the junction could be made <100 ps. With pulse forming circuits (Eckart *et al.* 1986) a single commercially available diode can produce 1.5 kV pulses into 50 Ω with pulse lengths as short as 100 ps. There is very little jitter in the avalanche breakdown time so the output from a single diode and its pulse forming network can be combined with other diode pulse formers to drive several gated detector areas.

The advantage of reverse biased *p-n* junctions over Auston switches is that there is no need for a very fast laser pulse to drive an Auston switch. Compared to laser triggered spark gaps, the diodes can be repetitively pulsed at about one kHz, allowing a sampling oscilloscope to be used for set up and testing of the cameras.

Gated microchannel plates are housed in gating modules which contain the phosphor and the vacuum feedthrough (Koenig 1988). The most convenient widths of microstrip transmission line coated onto 0.5 mm thick (L) Galileo microchannel plates, are 6 or 15 mm, with impedances of 12.5 and 6.25 Ω, respectively. Although a 15 mm wide microstrip is more attractive than 6 mm, the 40 mm diameter of convenient commercially available plates, the higher power needed to switch a lower impedance line and the high spatial resolution of the gated MCP detector (much less than 100 μm) results in 6 mm wide microstrips being most commonly used.

The maximum useful dimension of an image on a gated detector in the pulse propagation direction is set by the condition that either side of the image is recording data at time differences smaller than a fraction of the MCP gate time, e.g., $0.3 \times t_{gate}$. This restricts the useful length to $0.3\ V_p t_{gate}$ where V_p is the voltage propagation velocity along the microstrip. The velocity of propagation of a voltage wave on the microstrip is 15 mm/100 ps (~c/2), the FWHM of the fastest useful voltage pulse on $L = 0.5$ mm plates is ~160 ps, and the corresponding FWHM of the gain is $t_{gate} = 100$ ps, which gives a maximum length of image along the microstrip of ~5 mm.

The simplest configuration that produces multiple images on a single MCP has the microstrips parallel to each other as shown in figure 8(a). Images placed 1.5 cm apart along each strip will have a time difference of 100 ps. Three 12 Ω microstrips can be accommodated without interference on a 40 mm diameter MCP, and several images can be placed on each of three 12 Ω microstrips. The disadvantage of this arrangement is the large number of vacuum feedthroughs required, and the high power when each of the four separate microstrips is individually gated. Furthermore, the relative timing of the gate pulses on microstrips could be hard to establish if the microstrips were fed from different pulse generators whose relative timing varied from shot to shot.

An alternative configuration represented in figure 8(b) reduces the gating power requirement by doubling the switching voltage by open circuit reflection. In this case the four gating areas are arranged at the corners of a rectangle (Kilkenny 1988). The gating pulse is split into four, with each one being fed into one gating area. This scheme efficiently uses the gating power available, but leads to a nonuniform response with a scalelength of the propagation distance of the voltage pulse during the voltage FWHM. This gain non-uniformity is calculable from a superposition of the incident and reflected voltage pulse with appropriate time differences. Only at the open circuit end does voltage doubling occur, with voltages less than 2 V resulting from summing the incoming and reflecting pulse away from the end. The calculated and measured field nonuniformity is shown in figure 9.

This gated detector arrangement has been used both on the Nova laser at LLNL (Kilkenny 1989) and the Omega laser at LLE (McCrory 1989) to record the time evolution of implosions. By using four X-ray pinholes to project a different X-ray image onto each

detector, a sequence of imploding images with 100 ps gate times separated by 200 ps is obtained. Figure 10 shows an implosion sequence from a directly-driven target where one side of the target was irradiated first. The X-ray emitting shell is seen in the first two frames before stagnation, and a stagnation implosion core is seen on frame three with an expan-

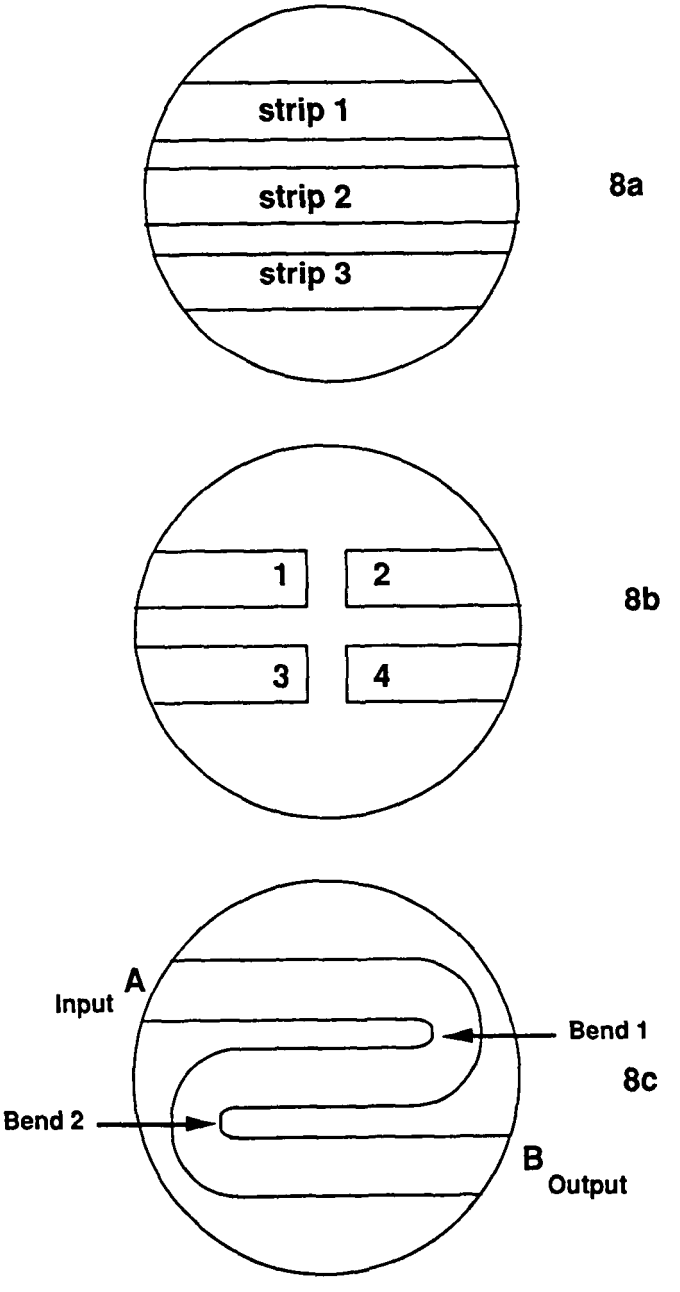

FIGURE 8. Some configurations of microstrips coated onto MCPs that have been used to detect multiple gated X-ray images. In (a) voltage pulse is propagated across the three strips. In (b) four separate pulses propagate along each microstrip and double up at the open circuits ends of each microstrip. In (c) a single pulse propagates along a meander microstrip with a time difference between input and output of typically 1 ns.

https://doi.org/10.1017/S0263034600002330 Published online by Cambridge University Press

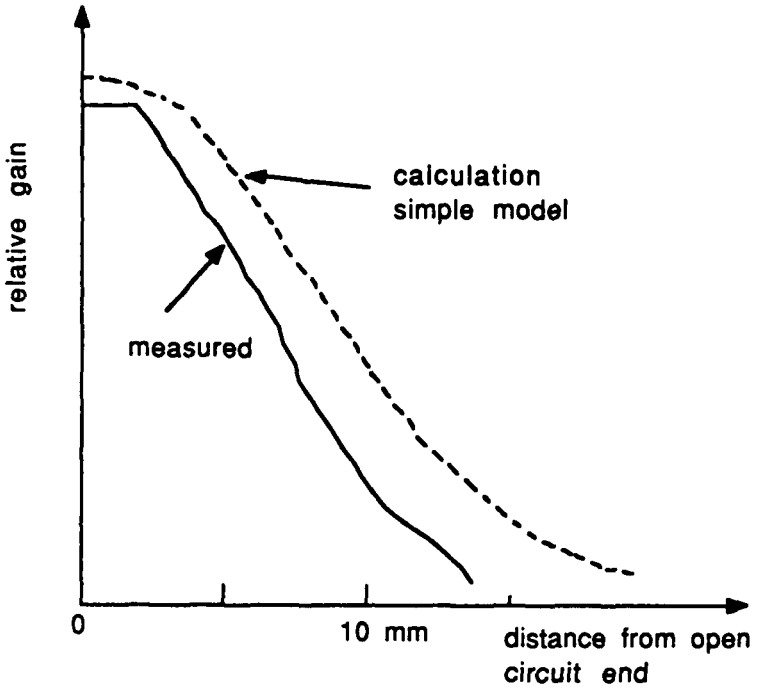

FIGURE 9. The calculated and measured non-uniformity in gain close to the end of an open circuit microstrip detector. This is the configuration used in one sector of figure 8(b). For the case illustrated here, a 200 ps FWHM pulse was used.

sion on the last frame. From images such as these, temporal and spatial properties of implosions are being examined. These instruments have become crucial in demonstrating good drive uniformity of implosions.

This layout has been routinely used for implosion measurements at Lawrence Livermore National Laboratory and the University of Rochester on implosion experiments on the Nova and the Omega lasers, respectively. This scheme has the disadvantages of requiring many feedthroughs and a nonuniform response.

A novel configuration used recently (Bell 1989) results from coating a single microstrip in a meander as shown in figure 8(c). The 6 mm wide strips are separated by 3.5 mm to avoid cross talk and to minimize reflections at the corners. A single voltage pulse enters at point A, propagates the length of the meander strip exiting at point B. With the geometry illustrated in figure 8(c), the effect of reflections at the bends are small. This configuration could be achieved with layout 1a by external cables connecting the ends of three separate strips; however, the need to make the cable connection outside the mechanical housing would imply a large time delay and some loss of fidelity between the ends of successive strips.

In use as a gated X-ray camera (Bell 1989), 14 X-ray images were projected by a 14 aperture pinhole onto the meander microstrip with an image spacing of 7.4 mm. The 150 ps voltage pulse propagates along the serpentine sequentially turning on each image, with delays of 50 ps. The camera was filtered to 2 keV photons and used to take a series of images of a direct-drive implosion on the Omega laser at the University of Rochester. The target for this image was a deuterium filled glass shell of about 250 μm diameter with 5 μm wall thickness imploded by uniform irradiation by a 650 ps, 0.35 μm, 1.2 kJ, 24 beam la-

https://doi.org/10.1017/S0263034600002330 Published online by Cambridge University Press

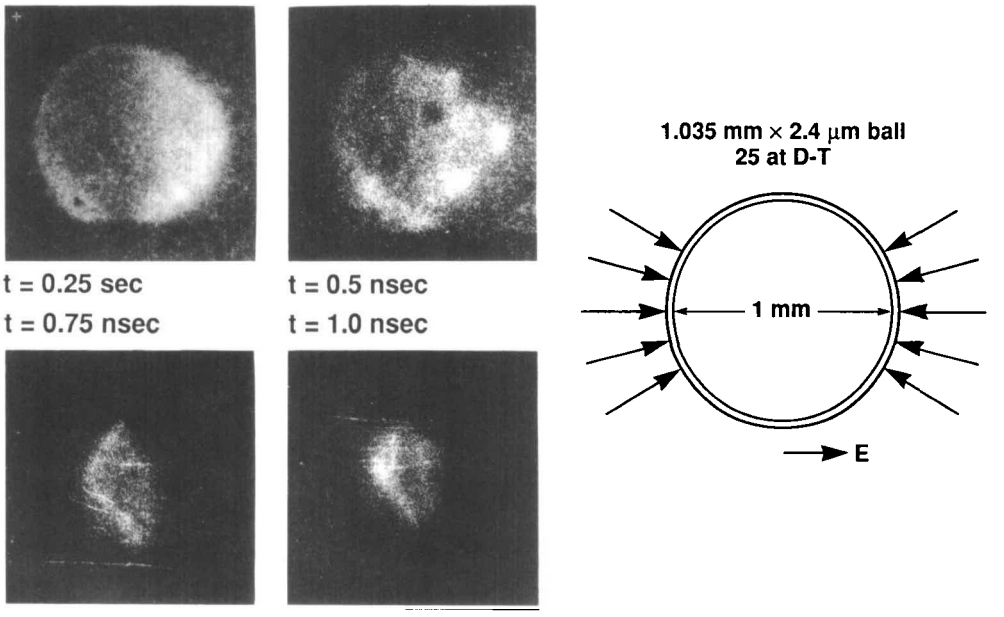

FIGURE 10. A sequence of 100 ps gated X-ray images during the implosion by direct irradiation of a glass capsule.

ser. Results are shown in figure 11. The initial images show the shell of X-ray emission from the glass heated by the laser irradiating. By the fourth frame, the ball has clearly started to implode. By the ninth frame, an implosion core, formed by the gaseous fuel becomes visible. The implosion continues reaching a minimum size by the final frame.

In figure 11, the advantages of many frames are evident. The separation in time of the images is 50 ps compared to a gate time of 100 ps. There is as much information on the image as a one-dimensional streaked image, but there is the added advantage of two-dimensional imaging.

In figure 11 the imploded image is several times brighter than the images at early time. It is fortunate that the increase in brightness of the image at late time is compensated by the drop in sensitivity of the detector due to the coating resistivity causing the amplitude of the gating voltage to drop. Schemes to minimize the resistivity loss are being investigated. An alternative approach would be to taper the width of the line thereby increasing the characteristic impedance as such that the gating voltage remains constant.

5. Future developments in proximity gating

5.1 *Vacuum gap systems*

Proximity focused schemes using a vacuum gap and an MCP collimator (Stearns *et al.* 1989) have produced gate times as short as 40 ps (Stearns 1989). The limitation is the gat-

https://doi.org/10.1017/S0263034600002330 Published online by Cambridge University Press

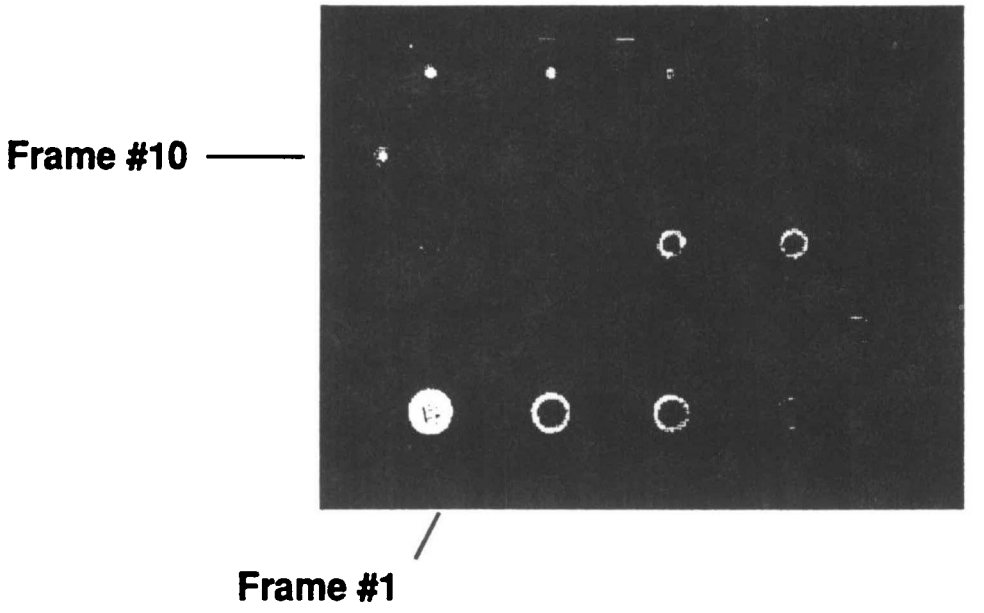

FIGURE 11. A sequence of images separated by 50 ps of an imploding glass capsules. The 250 μm glass microballoon was imploded by a 650 ps FWHM laser pulse. The shell can be seen imploding from frame #2. The central core starts to form at frame #8 (350 ps), the minimum size being seen at frame #13.

ing pulse which is presently produced by a 20 ps, 250 μJ light pulse activating an Auston switch. Although the switching time is of the order of the width of the optical trigger, the pulse that is generated contains high frequency oscillations from the lumped inductance and capacitance of the Auston switch. For the switch presently used, the rise time is ~12 ps and the characteristic damping time of ringing 4ZC is 50 ps.

Decreasing the microstrip gap from 1 mm to 200 μm (Stearns 1989) would reduce Z from 15 to 3 Ω. Although there is a necessary reduction in the gating voltage to prevent electrical breakdown, fast gating could still, in theory, be obtained.

Further improvements in the shutter times of proximity focus MCP devices also seem feasible, down to a shutter time of ~30 ps. The advantage is that there is a much less stringent voltage requirement allowing compact electronic generators to be used; the disadvantage is the restricted dynamic range because of MCP saturation effects.

For an MCP system the gate time is related to the electron transit time t_{tr} (eq. 4). For appreciable gain the voltage FWHM must not be less than t_{tr}, and the gate time is then $\sim t_{tr}/\gamma^{1/2}$. As

$$t_{tr} = \left(\frac{2m}{eV\beta}\right)^{1/2} L\left(\frac{L}{D}\right)^{1/2}$$

the combination of reducing L/D and L gives a lower value for t_{tr} as illustrated in Table 2. Also, a smaller L/D reduces the gain for a given voltage, allowing a higher voltage to be used without running the MCP into saturation. The higher voltage also reduces t_{tr}. This is illustrated in figure 12, where the MCP gain for various aspect ratio plates is plotted; an $L/D = 20$ MCP could be run at $V = 1400$ before saturation occurs. The gate times expected for various values of L/D and L of commercially available plates is shown in Table 2. An $L/D = 20$, L = 25 mm plate should give a gate time of 30 ps, from an electrical pulse

https://doi.org/10.1017/S0263034600002330 Published online by Cambridge University Press

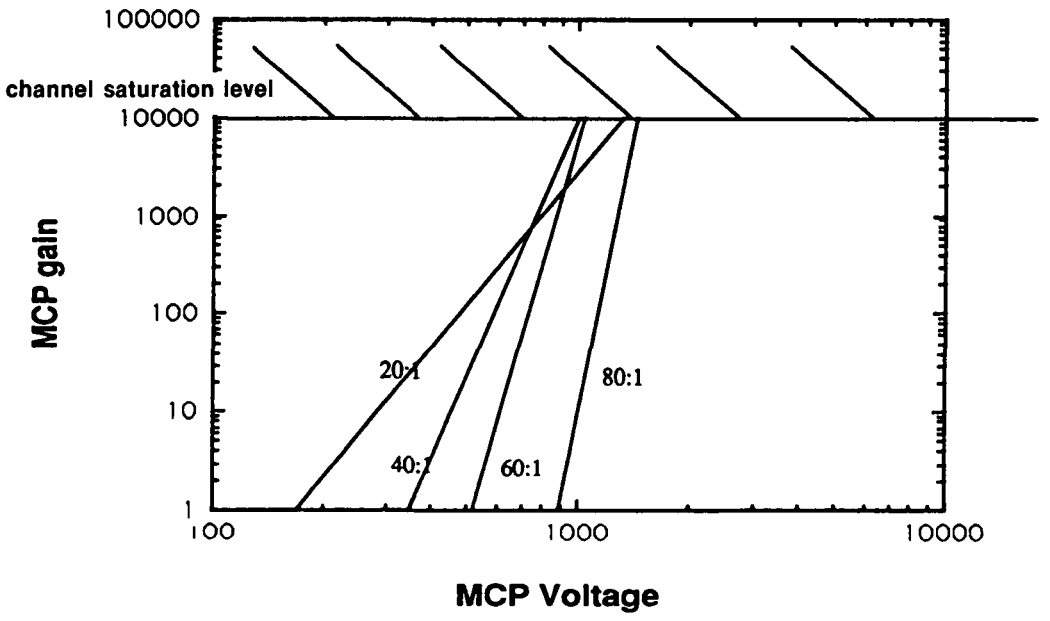

FIGURE 12. The MCP gain for various aspect ratios (L/D) MCPs. As an MCP gain in excess of 10^4 would cause channel saturation, there is an upper limit to the usable gate voltage of an MCP. The advantage of a lower L/D MCP is that a higher voltage could be used, resulting in a shorter gate time.

TABLE 2. Simple estimates of gate time can be made from $t_{tr} = (2m/\beta eV)^{1/2} L (L/D)^{1/2}$

L (mm)	(L/D)	γ	$V(\text{gain} = 10^4)$ (volts)	$t_{tr} = t_v$ (ps)	$t_g = t_{tr}/\gamma^{1/2}$ (ps)
0.5	40	10	980	240	76
0.25	40	10	1000	120	38
0.25	20	5	1400	70	31

FWHM of 70 ps. Such an electrical pulse is readily available from the avalanche breakdown of Si diodes.

In the near future, gate times of 20–30 ps with spatial resolution of much better than 10 lp/mm may become commonly available.

Acknowledgments

This work was performed under the auspices of the U.S. Department of Energy by the Lawrence Livermore National Laboratory under contract No. W-7405-ENG-48. I want to thank P. E. Bell, R. E. Booth, G. E. Power, R. Stewart and J. D. Wiedwald for many stimulating discussions; and R. Bonner and R. S. Thoe for some of the measurements quoted.

REFERENCES

AUSTON, D. H. 1976 *SPIE* **94**, 78–82.

BELL, D. A. 1960 *Electrical Noise* (D. Van Norstrands, London).

BELL, P. E. 1989 *SPIE* to be published.

BENZEL, D. M. & POCHA, M. D. 1985 *Rev. Sci. Instrum.* **56**, 1456.

COLE, A. J. *et al.* 1981 Rutherford-Appleton Laboratory, Annual Report No. RL-040-1981 (unpublished).

CSORBA, I. P. 1979 *App. Opt.* **18**, 2440.

DYMOKE-BRADSHAW, A. K. L. 1988 Private communication.

EAGLES, R. T., SIBBETT, W. & SLEAT, W. E. 1986 *Optics Comm.* **57**, 423.

EBERHARDT, P. 1979 *Applied Optics* **18**, 1418.

ECKART, M. J. *et al.* 1986 *Rev. Sci. Instrum.* **57**, 2046.

FARNSWORTH, P. T. 1930 U.S. Patent 1969399, filed March 30, 1930.

FEHL, D. L. *et al.* 1980 *Rev. Sci. Instrum.* **51**, 292.

FINN, N., HALL, T. A. & MCGOLDRICK, E. 1985 *App. Phys. Lett.* **46**, 731.

FLEUROT, N. *et al.* 1982 *SPIE*, **348**, 772.

GREKHOK, I. V. *et al.* 1981 *Prib. Tekh, Eksp.* **4**, 135.

HADLAND, R. 1978 *Proc. of 13th International Congress on High Speed Photography and Photonics*, Tokyo, 371.

HARES, J. D. 1987 *SPIE*, **831**, 165.

HENKE, B., KNAUER, J. D. & PREMARATRE, K. 1981 *J. Appl. Phys.* **52**, 1509.

ITO, M., KUME, H. & OBA, K. 1984 *IEEE Transactions on Nuclear Science*, **NS-31**, 408.

JACOBY, B. A., KOTECKI, D. E. & LEAR, R. D. 1983 *IEEE Transactions on Nuclear Science*, **NS-30**, 4624.

KALIBJIAN, R. & THOMAS, S. W. 1983 *Rev. Sci. Inst.* **54**, 1626.

KILKENNY, J. D. *et al.* 1988 *SPIE*, **913**, 147.

KILKENNY, J. D. *et al.* 1989. Proceedings of the Twelth International Conference on Plasma Physics and Controlled Nuclear Fusion Research, **Vol 3**, p. 29, IAEA, Vienna.

KILKENNY, J. D. *et al.* 1989a *SPIE* to be published.

KOENIG, Z. M. 1988 *Rev. Sci. Instrum.* **59**, 1813.

KOSHIDA, N. 1986 *Rev. Sci. Instrum.* **57**, 354.

KUME, H. *et al.* 1988 *Applied Optics* **27**, 1177.

LEONOV, N. B. & FYUTIKOV, A. M. 1980 *Pribory, Tekhnika Eksperimental* **1**, 193.

MATTHEWS, D. L. *et al.* 1985 *Phys. Rev. Lett.* **54**, 110.

MCCRORY, R. E. *et al.* 1989 Proc. 12th Int. Conf. on Plasma Physics and Controlled Nuclear Fusion Research, to be published, IAEA, Vienna.

MOROU, G., & KNOX, W. 1979 *Appl. Phys. Rev.* **35**, 7.

NAHRATH, B., SHAKHATRE, M. & DECKER, G. 1976 *Rev. Sci. Instrum.* **47**, 88.

POWER, G. & BELL, P. E. 1988 *SPIE*, **981**, 166.

PRICE, R. H., & WIEDWALD, J. D. 1983 Private communication, UCRL 89569.

SCHMIDT, K. C. & HANDEE, G. F. 1966 *IEEE Transactions on Nuclear Science*, **100**.

SIBBETT, W., RAGGS, M. R. & NIU, H. 1982 *SPIE* **348**.

SIBBETT, W. *et al.* 1989. SPIE, **406**, 406–414.

STEARNS, D. 1989 Private communication.

STEARNS, D. G. *et al.* 1986 *Rev. Sci. Instrum.* **57**, 2455.

STEARNS, D. G. *et al.* 1989 *Rev. Sci. Instrum.* **60**, 363.

STEWART, R. E. *et al.* 1983. unpublished, University of California, Lawrence Livermore National Laboratory Report No. UCRL-88580; Stewart, R. E. 1983, Ph.D. thesis, University of California.

WHEELER, H. A. 1977 *IEEE Transactions on Microwave Theory and Techniques (MTT)* **25**, 631.

WIZA, J. L. 1979 *Nuclear Instruments and Methods* **162**, 587.

YATES, G. J. *et al.* 1986 *SPIE* **693**, 57.

YOUNG, B. K. *et al.* 1986 *Rev. Sci. Instrum.* **57**, 2729.

YOUNG, B. K. *et al.* 1988 *Proceedings of the SPIE* **1118**, 913.